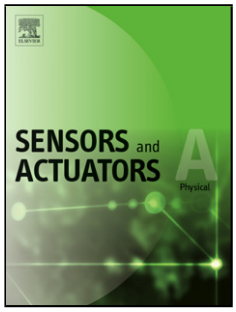

Title: Improvement of unidirectional focusing periodic permanent magnet shear-horizontal wave electromagnetic acoustic transducer by oblique bias magnetic field

Authors: Hongyu Sun, Songling Huang, Qing Wang, Shen Wang, Wei Zhao

PII: S0924-4247(18)31835-1
DOI: https://doi.org/10.1016/j.sna.2019.03.003
Reference: SNA 11271

To appear in: *Sensors and Actuators A*

Received date: 29 October 2018
Revised date: 24 February 2019
Accepted date: 3 March 2019

Please cite this article as: Sun H, Huang S, Wang Q, Wang S, Zhao W, Improvement of unidirectional focusing periodic permanent magnet shear-horizontal wave electromagnetic acoustic transducer by oblique bias magnetic field, *Sensors and amp; Actuators: A. Physical* (2019), https://doi.org/10.1016/j.sna.2019.03.003

Improvement of unidirectional focusing periodic permanent magnet shear-horizontal wave electromagnetic acoustic transducer by oblique bias magnetic field

Hongyu Sun[1], Songling Huang[1]*, Qing Wang[2], Shen Wang[1], Wei Zhao[1]

[1]*State Key Lab. of Power System, Department of Electrical Engineering, Tsinghua University, Beijing, 100084, China.*
[2]*Department of Engineering, Durham University, Durham, UK.*
* Correspondence to: Songling Huang. (E-mail: huangsling@tsinghua.edu.cn)

Graphical abstract

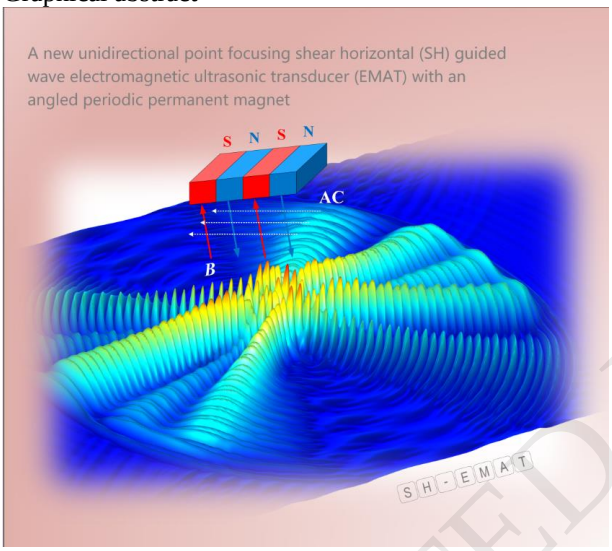

Highlights

- In this manuscript, a new unidirectional SH wave EMAT with oblique permanent magnet for the inspection of the aluminum plate is presented for the first time. The oblique angle of the permanent magnet enhances the guided signal on one side and weakens the ultrasonic signal on the other side. Therefore, the angled bias magnetic field can improve the focusing ability of the SH guided wave transducers effectively. It is concluded that the oblique PPM can improve the focusing ability of the unidirectional point-focusing SH guided wave EMAT and suppress the influence of the reflected signal, and then improve the resolution of the ultrasonic signal at the focusing point. In the study of the influence of the oblique angle of the permanent magnet on the focusing SH guided wave EMAT, the displacement amplitude at the focal point increases as the angle increases while the growth rate decreases. For the other side of the focal position, the displacement amplitude at that point decreases linearly as the angle increases.

Abstract: We propose a new unidirectional point focusing shear horizontal (SH) guided wave electromagnetic ultrasonic transducer (EMAT) with an angled periodic permanent magnet (PPM) in this work. The angled PPM developed here provides an angled bias magnetic field to achieve the EMAT's unidirectional focusing capability. The characteristics of the magnetic field distribution are analyzed by numerical and theoretical calculations. The simulation and experimental results are proven to be in good agreement when studying the bidirectional normalized amplitudes of the displacement of the single-coil SH-guided EMAT with oblique permanent magnets. Both the proposed angled transducer structure and the traditional paralleled transducer structure are performed and simulated using the three-dimensional Finite Element Method (FEM) to compare their unidirectional focusing capabilities. The results show that the SH guided wave EMAT of the focusing coils with an oblique permanent magnet enhances the signal on the focusing side and weakens the signal on the other side effectively. This performance can suppress the influence of the reflected signal from the unfocused side and further improve the ultrasonic signal's resolution. Moreover, it is shown in the

study that increasing the oblique angle of the PPM makes it difficult to increase the signal strength at the focal point when the angle reaches a certain value, but it is still effective at weakening the signal on the unfocused side.

Key words: Oblique periodic permanent magnet, SH guided wave, unidirectional focusing, point focusing, oblique angle

Declarations of interest: none

I. INTRODUCTION

The ultrasonic guided wave testing technique is more sensitive, economical, and convenient than conventional non-destructive testing (NDT) techniques [1–5]. The testing methods of ultrasonic guided waves can be divided into piezoelectric ceramics, magnetostriction, piezoelectric thin films, and electromagnetic ultrasonic testing according to different excitation modes [6–8]. The most widely used of the above methods is piezoelectric ultrasonic testing, which uses piezoelectric transducers for the excitation and reception of ultrasonic guided waves. Although piezoelectric ultrasonic technology has significant advantages and shows greater efficacy, the presence of the couplant can restrict the application of such a transducer in extreme environments, including the inspection's accuracy and efficiency. Therefore, the electromagnetic ultrasonic testing technique has excellent advantages in these aspects [9–14].

Ultrasonic guided wave technology has been widely used in the detection of large metal plates [15–17]. Due to the dispersion characteristics of ultrasonic guided waves and the characteristics of the different modes of ultrasonic waves, it is necessary to consider how the material performs when selecting an appropriate mode of ultrasonic guided wave for the plate inspection. The electromagnetic acoustic transducer (EMAT), which acts as an essential energy excitation and reception transducer in electromagnetic ultrasonic guided wave testing, relies on electromagnetic coupling to achieve the vibration of particles on the plate surface and wave propagation. However, the energy conversion efficiency of EMAT is much lower than that of conventional piezoelectric ultrasonic transducers, only about one percent. Since the energy signal is so weak, EMAT requires a high signal receiving circuit, a high signal-to-noise ratio (SNR), and high-gain operational amplifier is required to identify and amplify the extracted signal. Therefore, to increase the sensitivity and efficiency of the EMAT, the guided wave mode and structure of the transducer are required to be selected properly. Shear-Horizontal (SH) ultrasonic guided wave testing is a common detecting technology for metal plates, where the fundamental SH0 mode guided wave has been widely used in industry [18–22]. The SH0 guided wave has great advantages in the detection process as the group velocity is constant and does not change with the frequency [23–26]. Besides, when the SH0 mode guided wave encounters a defect in the process of propagation in the metal plate, the SH waves with mode conversion are hardly recognized and received by the reception transducer. This can be explained by the fact that the frequency region of the SH0 guided wave is appropriately selected and narrowband filtering of the signal processing module is performed at the reception transducer. The SH guided mode can be controlled when the frequency is relatively low and the analysis efficiency of the guided wave detection signal and detection efficiency of the metal plate guided wave are also improved. Furthermore, the SH wave does not produce any out-of-plane displacement in the particle, so the particle motion and wave propagation are not affected by the medium of the steel plate. Thus, SH guided wave is suitable for electromagnetic ultrasonic guided wave testing in metal plates.

At present, the mechanism of SH ultrasonic guided wave mainly includes the magnetostriction and the Lorentz force. Ribichini compared and analyzed the advantages and disadvantages of these two types of EMAT through experimental and numerical investigations and concluded that while ultrasonic transducers based on magnetostriction mechanisms could produce larger signal amplitudes, the use of magnetostriction coupling materials removed the non-contact characteristics of the transducers [27]. An SH guided wave EMAT that uses a periodic permanent magnet (PPM) in the detection of an aluminum plate is utilized in this study. The structure of the transducer includes a PPM and the coils excited by the alternating current. Therefore, due to the EMAT's low energy conversion efficiency, the strength of the signal can generally be improved by optimizing these two parts of the transducer. Song developed a focusable and rotatable SH Wave EMAT to improve the amplitude and directivity of the signals, which increased the energy conversion efficiency of the traditional transducers [28]. However, focusing such a signal is achieved by the cooperation of two rotatable transducers, so the configuration has a complicated structure that is both hard to control and expensive, and the signal's focusing effect is not particularly obvious. In practical applications, the size and blind area of multiple transducers are too large to utilize in aluminum plate defect detection. Ogi improved the coupling efficiency of the SH guided wave EMAT by changing the angle of the bias magnetic field based on magnetostriction theory [29]. However, the non-contact characteristics of the PPM EMAT meant that it was necessary to study the angle of the PPM EMAT in the specimen inspection. Therefore, it is significant to arrange the coils and permanent magnets reasonably to improve the detection signal' strength, which is the purpose

of this study.

In this work, we propose a new unidirectional point-focusing SH guided wave EMAT that uses a fan-shaped PPM with an oblique angle by comparison with the bidirectional and unidirectional three-parallel coils SH guided wave EMAT. The effect of the PPM's oblique angle on the unidirectional focusing of the ultrasonic signal is calculated using a 3-D model and verified by experiments. Then, the effect of the oblique permanent magnets on the amplitude of the SH guided waves that are generated by a single coil is investigated at different angles. This study also investigates the variation in the displacement at the focal point and the corresponding symmetrical position with the oblique angle of the bias magnetic field.

II. METHOD

A. Magnetic field calculation of the rectangular permanent magnet

Permanent magnets are critical in the generation of ultrasonic signals as a source of the bias magnetic field in the EMATs. The magnetic field of a finite-size permanent magnet can be regarded as a superposition of the magnetic field generated by magnetic charges. According to the theory of the equivalent magnetic charge, the magnetic field in space can be expressed as follows.

$$\boldsymbol{H} = \oint_S \frac{\sigma_{\mathrm{m}}}{4\pi\mu}\frac{\boldsymbol{r}}{r^3}\mathrm{d}S \tag{1}$$

where $\boldsymbol{H}$ is the magnetic field vector, σ_{m} is the surface magnetic charge density, μ is the magnetic permeability, $\boldsymbol{r}$ is the distance vector from the source point, S is the boundary of the permanent magnet.

According to the equation (1) and the schematic diagram of the rectangular permanent magnet shown in Fig. 1, the spatial magnetic field generated by the rectangular permanent magnet at each point can be obtained. In the coordinate system shown in Fig. 1, the magnetic field at point P(x, y, z) is

$$\boldsymbol{H} = \boldsymbol{H}_+ - \boldsymbol{H}_- = \iint_{S_+} \frac{\sigma_{\mathrm{m}}}{4\pi\mu}\frac{\boldsymbol{r}_+}{r_+^3}\mathrm{d}S - \iint_{S_-} \frac{\sigma_{\mathrm{m}}}{4\pi\mu}\frac{\boldsymbol{r}_-}{r_-^3}\mathrm{d}S \tag{2}$$

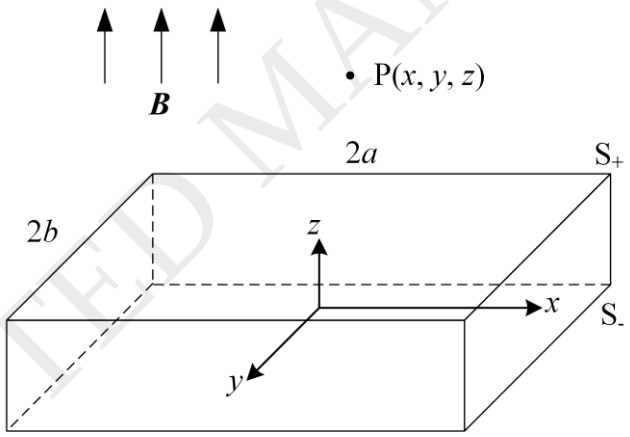

Fig. 1. Schematic diagram of the rectangular permanent magnet.

Although all the components of the magnetic field are not negligible in practice, in order to simplify the analysis in this study, since the transducer that generates the SH guided wave is based on the Lorentz force, the effective component of the magnetic field vector is considered to have only the z component. Moreover, the coil is located directly below the permanent magnet. Therefore, the solution of the magnetic field in the three directions can be simplified to that only in the z-direction.

$$\begin{aligned} H_{z+} = {} & \frac{B_{\mathrm{r}}}{4\pi\mu}\left[\arcsin\frac{(x-a)(y-b)}{\sqrt{(x-a)^2+z^2}\sqrt{(y-b)^2+z^2}} - \arcsin\frac{(x-a)(y+b)}{\sqrt{(x-a)^2+z^2}\sqrt{(y+b)^2+z^2}}\right] \\ & - \frac{B_{\mathrm{r}}}{4\pi\mu}\left[\arcsin\frac{(x+a)(y-b)}{\sqrt{(x+a)^2+z^2}\sqrt{(y-b)^2+z^2}} - \arcsin\frac{(x+a)(y+b)}{\sqrt{(x+a)^2+z^2}\sqrt{(y+b)^2+z^2}}\right] \end{aligned} \tag{3}$$

$$H_{z-}=\frac{B_r}{4\pi\mu}\left[\arcsin\frac{(x-a)(y-b)}{\sqrt{(x-a)^2+(z+h)^2}\sqrt{(y-b)^2+(z+h)^2}}-\arcsin\frac{(x-a)(y+b)}{\sqrt{(x-a)^2+(z+h)^2}\sqrt{(y+b)^2+(z+h)^2}}\right]-\frac{B_r}{4\pi\mu}\left[\arcsin\frac{(x+a)(y-b)}{\sqrt{(x+a)^2+(z+h)^2}\sqrt{(y-b)^2+(z+h)^2}}-\arcsin\frac{(x+a)(y+b)}{\sqrt{(x+a)^2+(z+h)^2}\sqrt{(y+b)^2+(z+h)^2}}\right] \tag{4}$$

Therefore, when the P(0, 0, *r*) point is known on the *z*-axis, the magnetic flux density is

$$B=B_z=\frac{B_r}{\pi}\left[\arcsin\frac{ab}{\sqrt{a^2+r^2}\sqrt{b^2+r^2}}-\arcsin\frac{ab}{\sqrt{a^2+(r+h)^2}\sqrt{b^2+(r+h)^2}}\right] \tag{5}$$

where B_r is the residual flux density of the permanent magnet, r is the coordinate of the z-axis, B_z is the magnetic flux density amplitude in the z-direction, $B_x=B_y=0$.

B. Physical model

In the calculation of the coupled electromagnetic field, the primary physical process can be described by the Maxwell equations.

$$\nabla\times\boldsymbol{H}=\boldsymbol{J} \tag{6}$$

$$\nabla\times\boldsymbol{E}=-\frac{\partial\boldsymbol{B}}{\partial t} \tag{7}$$

where $\boldsymbol{H}$ is the magnetic field; $\boldsymbol{J}$ is the current density; $\boldsymbol{E}$ is the electric field; $\boldsymbol{B}$ is the magnetic flux density. Moreover, Gauss's law for the electric field and magnetic field should be satisfied as follows.

$$\nabla\cdot\boldsymbol{D}=\rho \tag{8}$$

$$\nabla\cdot\boldsymbol{B}=0 \tag{9}$$

where ρ is the charge density. Two constitutive equations are utilized to solve the equations above:

$$\boldsymbol{D}=\varepsilon\boldsymbol{E} \tag{10}$$

$$\boldsymbol{B}=\mu\boldsymbol{H} \tag{11}$$

where ε is the dielectric constant and μ is the magnetic permeability.

Eddy current mainly exists in the skin depth of the specimen's surface, and the periodic Lorentz force is generated to excite the ultrasonic wave with the bias magnetic field. The dynamic magnetic field equation of the pulse eddy current is

$$\frac{1}{\mu}\nabla^2\boldsymbol{A}-\sigma\frac{\partial\boldsymbol{A}}{\partial t}+\frac{1}{S}\iint_s\sigma\frac{\partial\boldsymbol{A}}{\partial t}\mathrm{d}s=-\frac{\boldsymbol{i}}{S} \tag{12}$$

where $\boldsymbol{A}$ is the magnetic vector potential; σ is the conductivity of the material; $\boldsymbol{i}$ is the total current; S is the cross-sectional area of the coil conductor. The induced eddy current density is

$$\boldsymbol{J}_e=-\sigma\frac{\partial\boldsymbol{A}}{\partial t} \tag{13}$$

Also, the Lorentz force $\boldsymbol{F}_v$ will increase with the increase of the eddy current density.

$$\boldsymbol{F}_v=\boldsymbol{J}_e\times(\boldsymbol{B}_d+\boldsymbol{B}_s) \tag{14}$$

where $\boldsymbol{B}_d$ is the dynamic magnet flux density; $\boldsymbol{B}_s$ is the static magnetic flux density of the permanent magnet. Lorentz force plays a vital role as a coupling factor connecting the two models in the simulation.

The wave equation is shown which equals the Navier's equation in the isotropic elastic solid medium.

$$(\lambda+\mu)\nabla\nabla\cdot\boldsymbol{u}+\mu\nabla^2\boldsymbol{u}+\boldsymbol{F}_v=\rho\frac{\partial^2\boldsymbol{u}}{\partial t^2} \tag{15}$$

where $\boldsymbol{u}$ is the displacement vector; t the time; ρ the density; $\boldsymbol{F}_v$ the volume force vector which can be obtained from the calculation of the Lorenz force in the electromagnetic field model; λ and μ are the Lame's constants of the material.

C. Geometric model

In the Lorentz-based SH guided wave transducer, the applied bias magnetic field is generally along the normal direction of the aluminum plate surface, because this method can maximize the energy of the bias magnetic field to generate ultrasonic waves. Due to the bidirectional propagation characteristics of the SH guided wave, it is usually necessary to focus the signal on the detected side to improve the resolution of the signal while reducing the interference on the other side. Therefore, the direction of the bias magnetic field generated by the permanent magnet can be changed to achieve the unidirectional concentration of the signal.

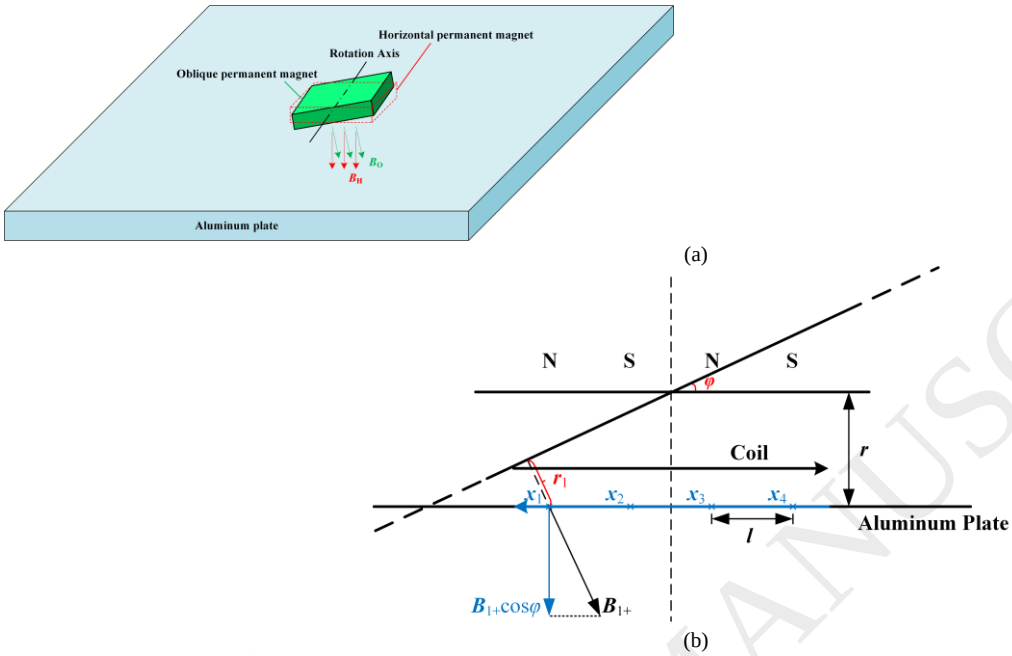

Fig. 2. Schematic diagram of the oblique permanent magnet EMAT: (a) Three-dimensional schematic diagram; (b) Two-dimensional geometry schematic diagram.

Fig. 2(a) shows the schematic diagram of the oblique permanent magnet EMAT proposed in this work. $\boldsymbol{B}_{\mathrm{H}}$ is the magnetic flux density produced by the horizontal permanent magnet while $\boldsymbol{B}_{\mathrm{O}}$ is produced by the oblique permanent magnet. In order to avoid the magnetostriction effect of the alternating magnetic field on the ferromagnetic material, the specimen is selected as an aluminum plate. Fig. 2(b) is a two-dimensional geometrical diagram that can analyze the principle of the oblique permanent magnet EMAT more intuitively from the perspective of analytical geometry.

Since the permanent magnet has a thickness h, in order to simplify the analysis process, the center of the lower surface of the permanent magnet can be regarded as the rotation axis. Then an angled bias magnetic field varies with the increase in the rotation angle φ of the periodic permanent magnet. Since the eddy current on the surface of the aluminum plate mainly exists on its surface, it can be assumed that the distance between the eddy current position and the periodic permanent magnet is r and the center distance of the different magnetic poles of the periodic permanent magnet is l. The wave velocity of the shear wave is a constant value, and the AC frequency applied on the coil is 1 MHz, and the phase superposition of the ultrasonic waves can be realized when the spacings of the SH guided wave radiation points are half wavelength, the spacings of the periodic permanent magnets is 1.6 mm in this study. Four points x_1, x_2, x_3, and x_4 are selected and located directly below each pole of the periodic permanent magnet, and on the surface of the aluminum plate, so the spacing between the adjacent points is 1.6 mm.

D. Numerical algorithm

As a multi-physical calculation & analysis software, COMSOL has excellent advantages in solving physical problems such as electromagnetic field coupled with the ultrasonic field in this study. The basic principle of the SH guided wave excitation by an EMAT is: The alternating eddy current generated by the alternating current in the coils causes the specimen to generate periodic vibration under the effect of the external bias magnetic field, thereby exciting and propagating the ultrasonic SH guided waves in two directions. Therefore, two modes in COMSOL are required to implement the simulation process: electromagnetic field and elastic dynamic field (also named as the solid mechanics' mode).

Using the numerical solution of Partial Differential Equation (PDE), the Finite Element Method (FEM) technique provides an approximate numerical method for solving the electromagnetic ultrasonic coupling problem. The algorithm utilized in the simulation includes solving the differential equations completely, or transforming the partial differential equation into an approximate system of ordinary differential equations, and then solving the numerical solution by Euler method. In the simulation, the joint solution method of three modes is mainly used for transient calculation. The magnetic field without current mode is mainly

implemented to calculate the bias magnetic field generated by the periodic permanent magnet. Moreover, the magnetic field module calculates the eddy current density induced by the alternating coil inside the aluminum plate. For the solution of the Lorentz force, the current density and magnet flux density calculated by the above two modes can be utilized to generate and propagate the ultrasonic waves in the solid mechanic's mode.

In the simulation, a three-dimensional model is used to analyze the generation and focusing characteristics of SH ultrasonic guided waves. It is significant to set the size of the grid cells when meshing the solution area. In order to ensure the accuracy of the eddy current calculation, at least seven grids should be ensured to be divided in the skin depth. Also, to ensure the accurate calculation of the ultrasonic SH waves, there should be at least seven grids in one wavelength. Therefore, in the simulation, the meshing of the computation domain is shown in Fig. 3 where the air domain is omitted and the meshing parameters are shown in Table 1. In the analysis of the simulation and experiment, except for particular explanations, the values of the parameters utilized are shown in Table 2 in this study.

The phase velocity of the SH0 mode wave does not change with the frequency-thickness product, and the SH0 wave mode has no dispersion. In order to utilize the characteristics of the SH0 mode guided wave, the following formula needs to be satisfied.

$$fd \le \frac{nc_T}{2} \tag{16}$$

In this work, the frequency is selected to be below the cut-off frequency for all modes n>0, and the thickness of the aluminum plate remains unchanged at 1 mm, and the transverse wave velocity in the aluminum plate is 3.2 km/s. Then the cutoff frequency of the SH1 mode guided wave is 1.6 MHz. Therefore, in order to obtain a pure SH0 mode guided wave, the drive frequency of the AC coil is selected as 1 MHz in the simulation and experiment.

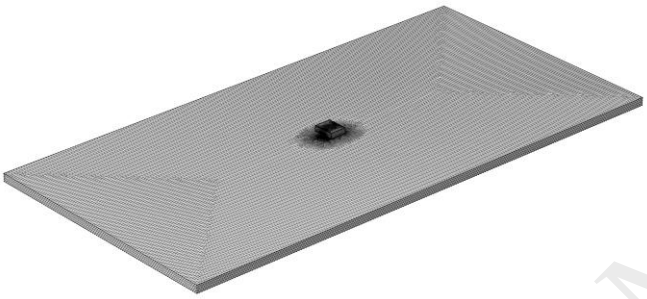

Fig. 3. The meshing of the computation domain.

Table 1
UNIT DIMENSION PARAMETER OF MESH GENERATION

Parameters	Value
Mesh vertices	1 206 434
Tetrahedron	7 091 087
Triangle	173 300
Edge element	2 444
Vertex element	28
Number of elements	7 091 087
Minimum unit quality	0.387
Average unit quality	0.975
Unit volume ratio	2.611×10^{-5}
Mesh volume (mm^3)	4×10^{6}

Table 2
PARAMETERS OF THE SH WAVE EMAT.

Parameters	Value
Focal radius (mm)	20
Lift-off distance (mm)	1
Lame's constants λ (GPa)	58
Lame's constants μ (GPa)	29
Aluminum specimen mass density (kg/m^3)	2 832
Aluminum specimen conductivity (S/m)	3.65×10^{7}

Remanent magnetism of the magnet (T)	1.21
Relative permeability of the magnet	400
Permanent magnet oblique angle (°)	20
Permanent magnet size (mm)	8×1.6×2

III. RESULTS

A. Magnetic field calculation of permanent magnets

In this section, we conduct a 3-D simulation using FEM in the COMSOL software for a rectangular permanent magnet, and the material parameters utilized in the simulation are shown in Table 2. The residual magnetic flux density of the rectangular permanent magnet is set to 1.21 T, and the direction of the vector is opposite to the normal direction of the aluminum plate. To validate the equation (5) through numerical simulation, Fig. 4(a) shows the vector distribution of magnetic flux density in the domain around the permanent magnet. It is shown in the figure that the closer to the permanent magnet surface and the permanent magnet edge, the larger the flux density vector exists. So near the center point of the permanent magnet such as P(0, 0, *r*), the magnetic flux density vector shows only the *z*-direction component, which is consistent with the method research above. Figure 4(b) shows a two-dimensional slice schematic of the magnetic flux density amplitude distribution. The eddy current density induced in the aluminum plate during the excitation of the high-frequency pulse current is shown in Fig. 4(c). It can be found that due to the edge effect, although the maximum value of the magnetic flux density appears at the edge position of the permanent magnet, the only contribution of the SH guided wave excitation is the *z* component of the magnetic field. Therefore, for such a simple rectangular permanent magnet, the corresponding relationship between magnetic flux density and distance can be obtained through numerical simulation and theoretical calculation by equation (5).

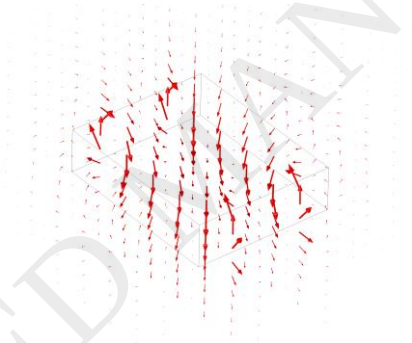

(a)

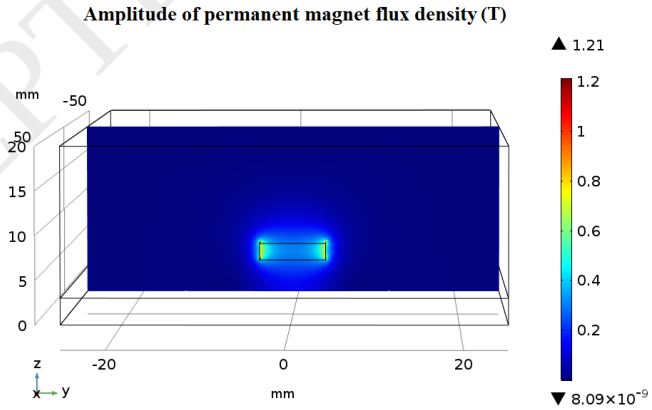

(b)

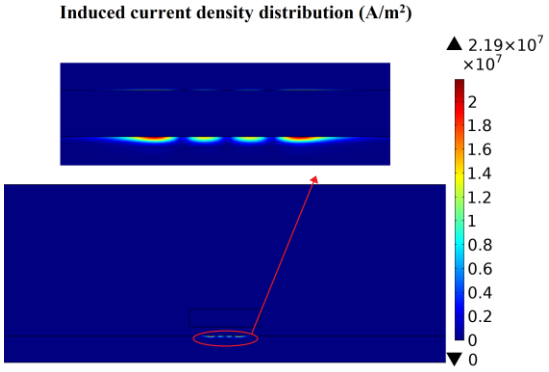

(c)

Fig. 4. Magnetic flux density calculation of permanent magnets: (a) 3-D vector schematic; (b) 2-D slice schematic; (c) The 2-D eddy current density distribution.

Fig. 5 shows a comparison between the simulation results and the analytical calculations under the same conditions and the calculated axis is located on the normal line at the center of the *x*-*y* plane of the permanent magnet, and it can be found that the two methods are highly consistent. It can be seen from the figure that as the distance in the *z*-direction increases, the magnetic flux density of the permanent magnet decreases nonlinearly. In the numerical solution of multi-physics problems, the description of the nonlinear problems by partial differential equations is accurate and reasonable. Therefore, it proves that the Finite Element Method is suitable for calculating the electromagnetic field of a simple geometry structure, and it makes it easier to solve the complex geometry that hard to obtain an analytical solution.

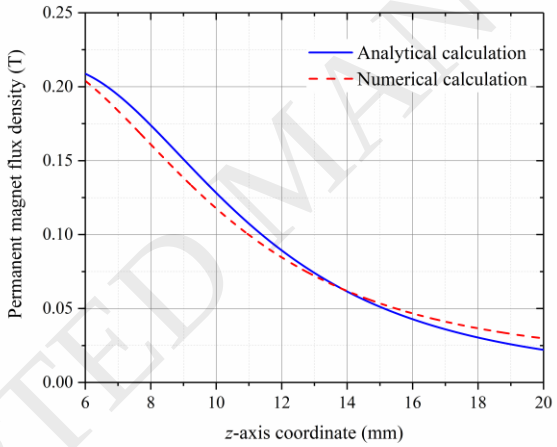

Fig. 5. Comparison of simulated and analytical solutions for the magnetic flux density of rectangular periodic permanent magnets.

B. Effect of the angled bias magnetic field by a single coil SH wave EMAT

In order to analyze the influence of the oblique permanent magnet on the excitation and propagation of the SH guided wave, it is assumed that there is only a single coil under the periodic permanent magnet. The points x_1, x_2, x_3 and x_4 on the surface of the aluminum plate shown in Fig. 2 represent the corresponding positions below the central points of each part of the periodic permanent magnet. When the permanent magnet is placed horizontally, for PPM with more permanent magnets, the magnetic flux densities at central positions of each magnet are approximately the same except for the permanent magnets on both sides. However, if the permanent magnet has an angle, the magnetic field between the points will be significantly different. Therefore, the magnitudes of the Lorentz forces at each point are different while the frequency remains the same.

Fig. 6(a) shows the time-varying Lorentz forces at x_1, x_2, x_3 and x_4 on the surface of the plate. In order to facilitate the comparison of the force at each point, normalization is used in this figure. The parameters utilized in the simulation refer to the values shown in Table 2, in which the oblique angle of the permanent magnet is set to 20 °. Therefore, it is shown in Fig. 6(a) that the magnitudes of the Lorentz forces at each point are different. Ultrasonic waves generated by the points with greater force are stronger while ultrasonic waves generated by the points with smaller force are weaker. Therefore, an asymmetrically distributed ultrasonic field can be obtained by tilting the bias magnetic field to achieve single-sided focusing of the ultrasonic guided wave signal.

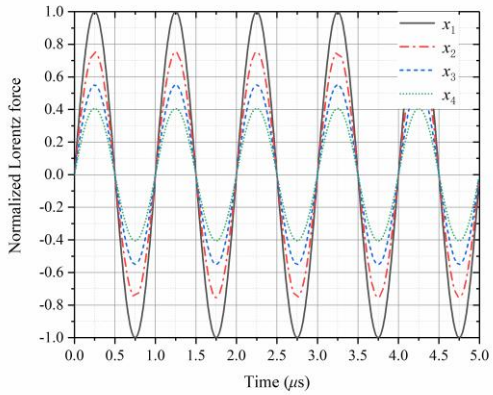

(a)

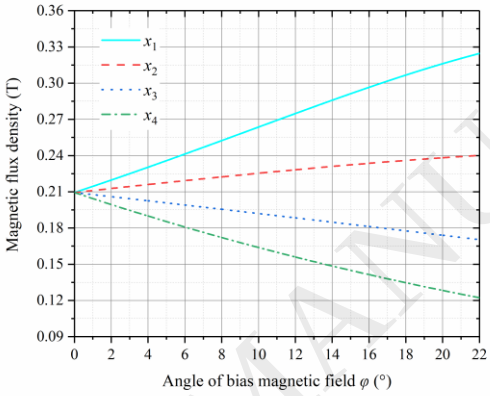

(b)

Fig. 6. The characteristics of the oblique permanent magnet at different positions such as x_1, x_2, x_3 and x_4 on the surface of the plate: (a) Time-varying Lorentz force at each point along the direction perpendicular to the wave's propagation direction at an angle of 20 °; (b) The effect of the oblique angle φ on the magnetic flux density at each point.

Since the angle φ of the permanent magnet affects the distribution of the ultrasonic field, it is necessary to analyze the magnetic flux density generated by the permanent magnets with different oblique angles at different positions, such as x_1, x_2, x_3, and x_4. As the rotation axis of the permanent magnet is assumed to be in the middle position herein, then as the angle φ increases, the magnetic flux density increases the fastest at x_1 while it becomes slower at x_2. The magnitude of the magnetic flux density at the x_3 and x_4 positions decreases as the oblique angle φ increases. It can explain the difference in the magnitude of the Lorentz force between different positions in Fig. 6(a).

Fig. 7(a-c) shows the displacement field distribution of the aluminum plate surface at different moments, in which the angle is 20 °. It can be seen that the SH ultrasonic guided wave propagates bidirectionally along the x-axis direction as time increases. In order to analyze the effect of the angled bias magnetic field on the ultrasonic wave propagation in detail, Fig. 7(d-f) shows the normalized displacement distribution at different moments along the x-axis direction. It can be seen from the figure that when the permanent magnet has an oblique angle, the displacement field distribution in the negative direction of the x-axis is 10% to 20% larger than that of the corresponding position on the other side. Therefore, the presence of the oblique permanent magnets can focus the signal on one side effectively.

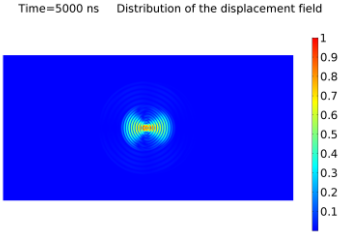

(a)

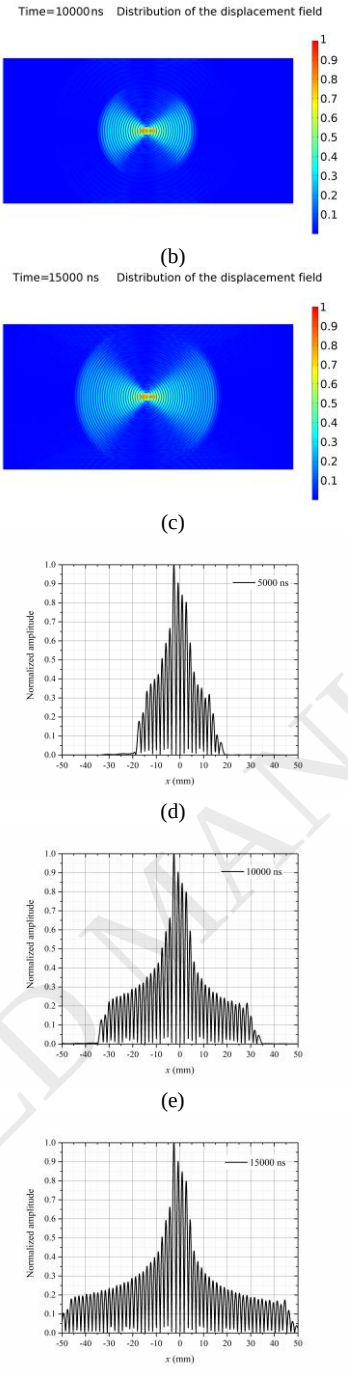

(b) (c) (d) (e) (f)

Fig. 7. Displacement field distribution under the angled bias magnetic field at different moments: (a, d) Displacement field distribution at 5000 ns; (b, e) Displacement field distribution at 10000 ns; (c, f) Displacement field distribution at 15000 ns.

In order to study the effect of permanent magnets with different oblique angles on the ultrasonic guided wave focusing capability, Fig. 8 shows the difference in the displacement amplitudes of the two symmetric coordinate points (±20 mm, 0) of the aluminum plate surface at different angles. It can be found that as the oblique angle increases, the difference in displacement amplitude between the focusing side and the unfocused side increases parabolically. It can be concluded that a larger permanent magnet angle can improve the effect of a unidirectional focusing EMAT. However, it should be noted that due to the geometry and insulation requirements, the angle has a maximum value which is related to the lift-off distance of the transducer and the size of the permanent magnet.

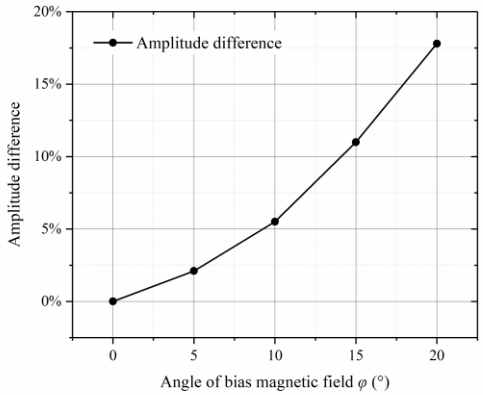

Fig. 8. The difference in the amplitude of the displacement amplitudes of the two symmetric coordinate points (±20 mm, 0) at different oblique angles of the permanent magnet.

C. Measurement

The aluminum plate used in the experiment is consistent with the simulation conditions in section B. Pulsed power (RPR 4000) is utilized in the experimental research in Fig. 9 to generate and receive signals. The power not only produces strong and stable sinusoidal high-frequency pulses but also identifies and receives the desired signals over a broad frequency band. The oscilloscope (TDS 1002) is utilized to display the waveform acquired by the RPR-4000, which has a bandwidth of 60 MHz and the sampling rate of 1 Gs/s. Impedance matching is achieved by connecting a 150-ohm resistor in parallel with the coil. To measure the magnetic flux density vector under the PPM magnet for validation purpose, we used a 3-D magnetic field measurement chip with three Hall sensors in three directions. Through three Hall probes, the components of the magnetic flux density at a certain point in space can be measured in the three directions of *x*, *y*, and *z*.

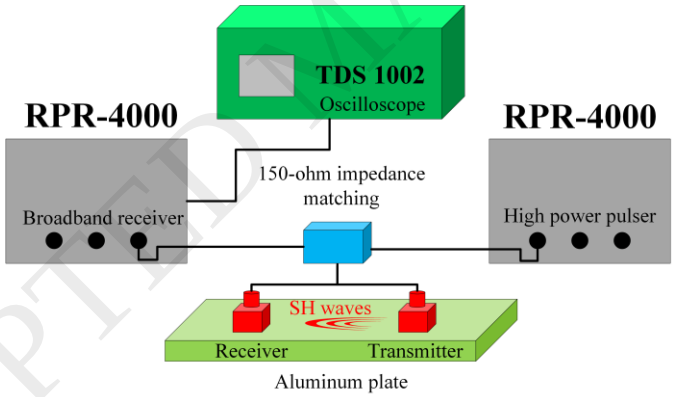

Fig. 9. Experimental configuration of oblique permanent magnet SH guided wave.

In order to compare with the simulation results, the oblique angle of the PPM used in the experiment can be adjusted within a certain range. The 3-D printing technology is utilized to obtain a wedge-shaped part with a fixed precise oblique angle to achieve the angular variability of the transducer. The non-magnetically conductive material used in printing is acrylonitrile-butadiene-styrene (ABS) to produce the required component. The comparison between the simulation results and the experimental results under the same conditions is shown in Fig. 10. The results have been normalized to make an intuitive comparison, and it can be found that the simulation results are in good agreement with the experimental results. Moreover, the maximum difference between the two values is less than 15%. The strong signal on the focusing side makes the detection of the defect more accurate while the weak signal on the unfocused side can effectively avoid the influence of the reflected signal on the signal extraction of the measurement point.

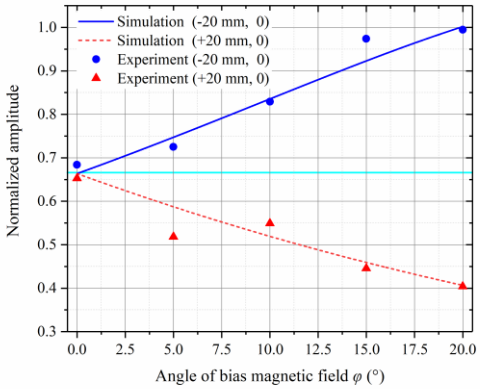

Fig. 10. The comparison between the simulation results and the experimental results at different angles of the permanent magnet.

IV. DISCUSSIONS

The oblique angle of the permanent magnet enhances the guided signal, and using the method above can improve the focusing ability of the SH guided wave transducers effectively. In the design of a conventional SH-guided EMAT structure, the coils are generally arranged in parallel, and the permanent magnets are placed horizontally above the plate. The arrangement of such a transducer structure can excite a bidirectional propagating SH guided wave and achieve a good phase superposition effect by adjusting the spacings of the periodic permanent magnets. However, this method can only detect defects in a specific direction, and the generated signal is relatively weak while the reflected signal on the other side also affects the resolution and extraction of the waveform. Therefore, in order to improve the unidirectional propagation characteristics of the ultrasonic guided waves and to achieve the point focusing ability of the EMATs, a novel transducer structure with oblique permanent magnets has been developed in this study.

A. The angled PPM with parallel coils

Fig. 11(a) shows the structural arrangement of the parallel coil horizontal permanent magnet SH ultrasonic guided wave EMAT and Fig. 11(b) shows the transducer structure with the oblique permanent magnet. In order to simplify the analysis process and facilitate comparison, three coils are utilized in the simulation to simulate a multi-coil transducer configuration. The spacings of the three coils are fixed to 3 mm and arranged symmetrically on the *x*-*y* plane. The excitation current in the coil is a sinusoidal AC with a frequency of 1 MHz. The horizontal permanent magnet has an angle of 0 °, and the oblique permanent magnet has an angle of 20 ° in the simulation.

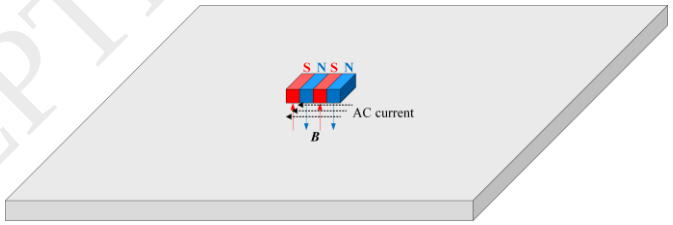

(a)

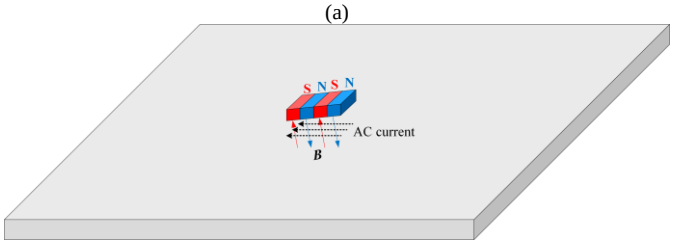

(b)

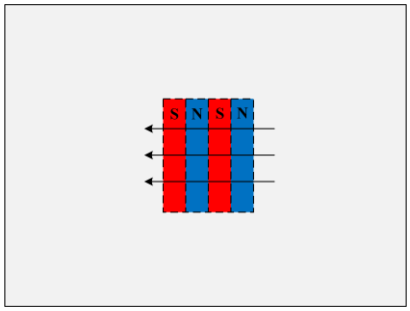

(c)

Fig. 11. Schematic diagram of the three-parallel coils SH guided wave EMAT configuration: (a) Horizontal periodic permanent magnet; (b) Oblique periodic permanent magnet with an angle of 20 °; (c) The coil structure.

Fig. 12(a) shows the distribution of the normalized displacement field at the moment of 15000 ns for the parallel coil EMAT with the horizontal permanent magnet. It can be found in the figure that due to the symmetrical configuration of the transducer structure, the calculated displacement field is also symmetrically distributed. The normalized displacement distribution of the surface of the aluminum plate in the *x*-axis direction of the symmetry axis is shown in Fig. 12(b). It can be found that the displacement component around the center point is the largest, and the displacement amplitude decreases gradually as the distance increases. There will be a transitional suppression zone before the guided wave is generated, so the amplitude of the displacement will be relatively small near this position.

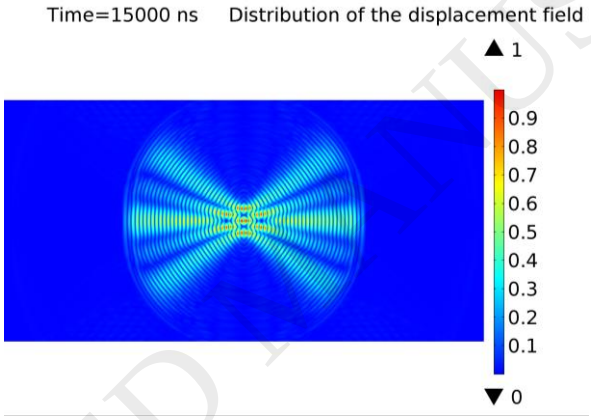

(a)

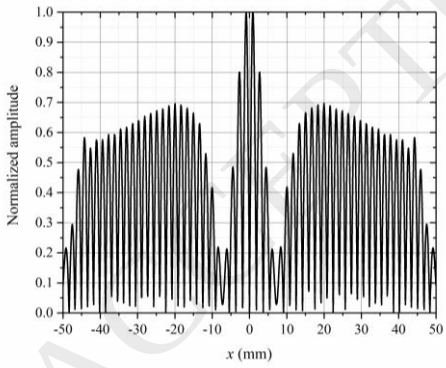

(b)

Fig. 12. Normalized displacement field distribution of three-parallel coils SH guided wave EMAT: (a) Two-dimensional schematic diagram; (b) Distribution along the *x*-axis on the surface of the aluminum plate.

When the permanent magnet has an oblique angle, the distribution of the displacement field will be affected. Fig. 13(a, b) shows the displacement field distribution at 15000 ns and the normalized displacement along the *x*-axis for the oblique permanent magnet with an angle of 20 °. It can be observed from the figure that the distribution of the displacement field is not symmetrically distributed along both sides of the propagation direction, but shows a larger displacement on the focusing side. Since the oblique permanent magnet causes uneven distribution of the Lorentz force amplitude on the plate surface, a difference in the amplitude of the ultrasonic wave at the radiant point is generated. The particle near the oblique side of the permanent magnet produces a large displacement while the particle away from the side of the permanent magnet leads to a small displacement. Therefore, the figure

shows that the displacement on the left side is higher than that of the right side, which can be explained by the rotation direction of the bias magnetic field. It can be seen that it is useful to set an angle of the permanent magnet to achieve unidirectional focusing of the signal. Moreover, compared with Fig. 7(a-f), it can be seen that the increase in the number of the coils improves the unidirectional focusing effect of the signal.

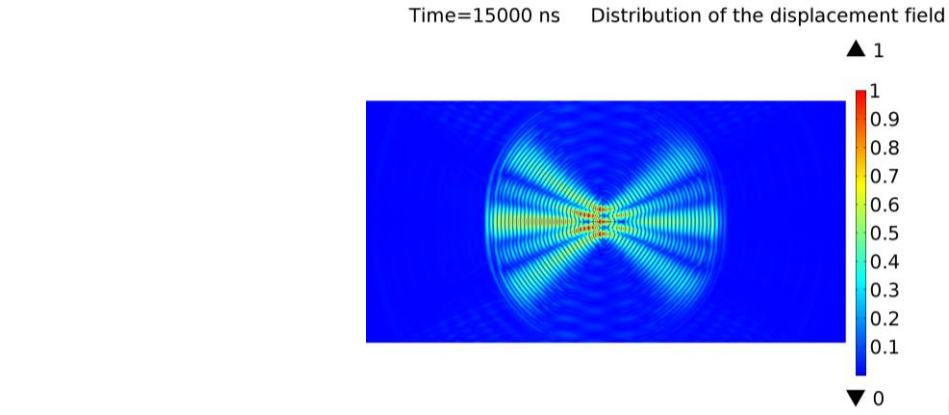

(a)

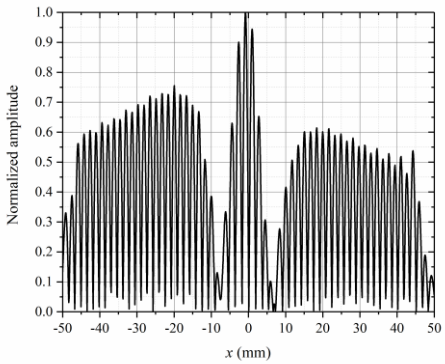

(b)

Fig. 13. Normalized displacement field distribution of three-parallel coils SH guided wave EMAT with an angled PPM: (a) Two-dimensional schematic diagram; (b) Distribution along the *x*-axis on the surface of the aluminum plate.

B. The angled PPM with focusing coils

Since the SH ultrasonic guided wave has a specific direction of the propagation, the direction of the coils can be directed to a certain point by rearranging the parallel coils in the transducers. In order to ensure that the ultrasonic waves generated by each coil also satisfy the phase superposition, it is necessary to design a fan-shaped periodic permanent magnet EMAT to improve the strength of the signal. The new transducer consists of a fan-shaped periodic permanent magnet with three centripetal coils while the center of the coil is defined as the focal point. The propagation direction of the SH guided wave excited by the Lorentz force is pre-determined as it propagates bidirectionally along the surface of the aluminum plate and perpendicular to the vibration direction of the shear waves. Therefore, the focal point of the three coils can also be regarded as the focusing position of the ultrasonic waves. In such a transducer configuration, unidirectional focusing characteristics of the signal can be achieved by using the fan-shaped permanent magnets with an angle. Fig. 14(a) shows the configuration of the SH guided wave EMAT with the horizontal fan-shaped permanent magnet while Fig. 14(b) shows the configuration with an angled PPM.

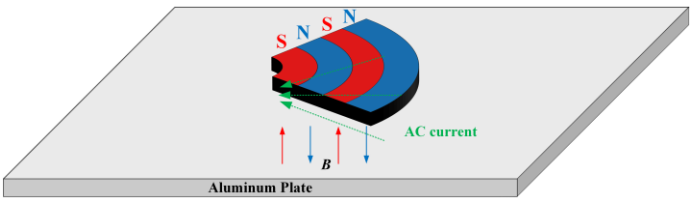

(a)

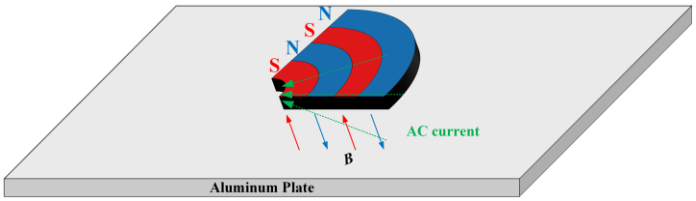

(b)

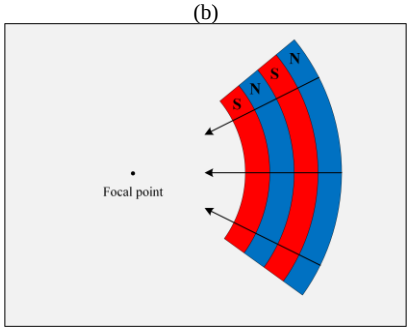

(c)

Fig. 14. Schematic diagram of the point-focusing coils SH guided wave EMAT configuration: (a) Horizontal periodic permanent magnet; (b) Oblique periodic permanent magnet with an angle of 20 °; (c) The coil structure.

In the simulation, the aperture angle of the focusing coils is set to 40 ° and the center-to-center spacing of the coils is also 3 mm in order to facilitate the comparison with the parallel coil EMATs. The position of the focal point is predefined as (-20 mm, 0) on the aluminum plate. Fig. 15(a) shows the normalized displacement field distribution and Fig. 15(b) shows the distribution along the surface of the *x*-axis aluminum plate. It can be seen that the magnitude of the displacement at the focal point is much larger than the displacement of the position other than the point of the radiation source. Fig. 16 (a, b) shows the normalized displacement field distribution of a point-focusing SH guided wave EMAT with an angled bias magnetic field. It can be seen from the figure that the displacement at the focal point is enhanced while the displacement on the unfocused side is weakened. This proves that the presence of the oblique PPM can improve the focusing ability of the unidirectional point-focusing SH guided wave EMAT, and then improve the resolution of the ultrasonic signal.

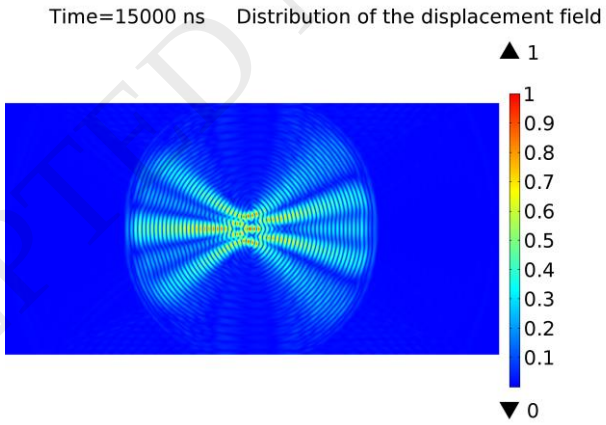

(a)

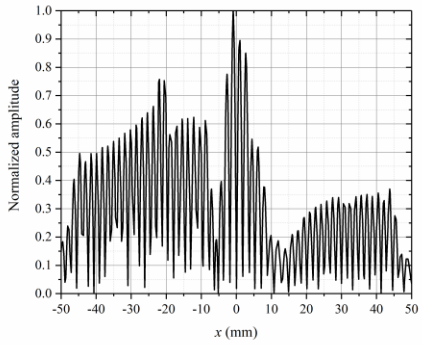

(b)

Fig. 15. Normalized displacement field distribution of the point-focusing coils SH guided wave EMAT: (a) Two-dimensional schematic diagram; (b) Distribution along the *x*-axis on the surface of the aluminum plate.

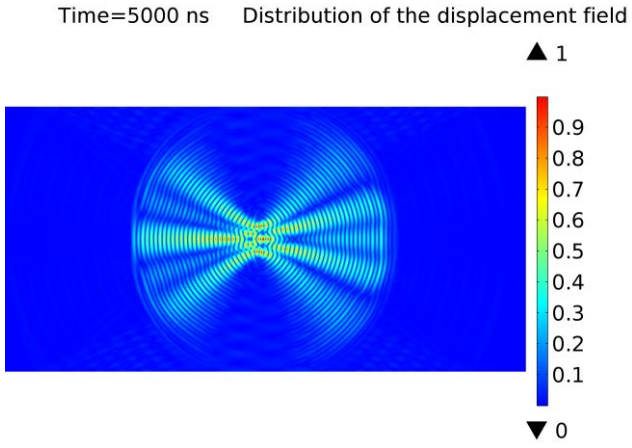

(a)

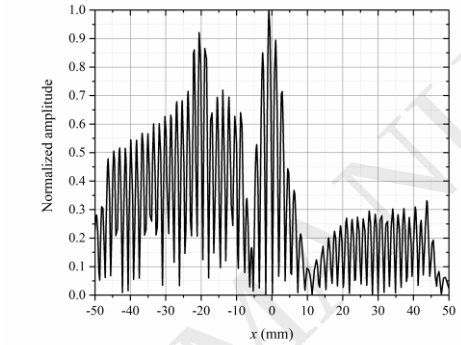

(b)

Fig. 16. Normalized displacement field distribution of the point-focusing coils SH guided wave EMAT with an angled PPM: (a) Two-dimensional schematic diagram; (b) Distribution along the *x*-axis on the surface of the aluminum plate.

To investigate the effect of the angle of the biasing magnetic field on the unilateral point focusing, Fig. 17 shows the effect of different angles on the normalized displacement at the focal point (-20 mm, 0) and its corresponding point (20 mm, 0) on the other side. It can be found that as the oblique angle of the magnetic field increases, the displacement at the focal point increases while the rate of growth gradually decreases when it reaches 1. At the non-focus side at (20 mm, 0), the displacement amplitude at that point decreases approximately linearly as the angle increases. Therefore, increase the oblique angle of the permanent magnet will make it hard to enhance the signal strength at the focus point when the angle reaches a certain value, but it is still effective to weaken the signal on the unfocused side.

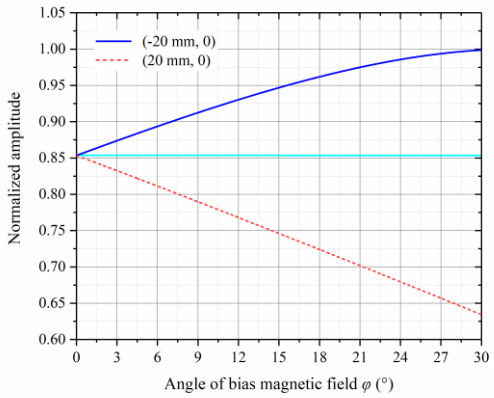

Fig. 17. Effect of different angles on the normalized displacement at the focal point (-20 mm, 0) and its corresponding point (20 mm, 0) on the other side

V. CONCLUSIONS

In this work, a new unidirectional SH wave EMAT with the oblique permanent magnet for the detection of the aluminum plate is presented. For the single coil EMAT, the experimental and simulation results are in good agreement. It indicates that the increase in the bias magnetic field angle leads to an increase in the EMAT's unidirectional focusing ability. The oblique angle of the permanent magnet enhances the guided signal on one side and weakens the ultrasonic signal on the other side. Therefore, the angled bias magnetic field can improve the focusing ability of the SH guided wave transducers effectively. For a single coil EMAT, the use of an angled PPM increases the signal strength on the focusing side by 10% to 20%, and the focusing capability will be further enhanced through the increase in the coil number. To study the role of permanent magnet oblique angle in the conventional transducers and new focusing transducers, two different transducer structures with parallel coils and focusing coils are simulated and analyzed in this study. It is concluded that the oblique PPM can improve the focusing ability of the unidirectional point-focusing SH guided wave EMAT and suppress the influence of the reflected signal, and then improve the resolution of the ultrasonic signal at the focusing point. In the study of the influence of the oblique angle of the permanent magnet on the focusing SH guided wave EMAT, the displacement amplitude at the focal point increases as the angle increases while the growth rate decreases. For the other side of the focal position, the displacement amplitude at that point decreases linearly as the angle increases.

ACKNOWLEDGMENTS

This research was supported by the National Key R&D Program of China (Grant No. 2018YFF0214701), National Natural Science Foundation of China (NSFC) (No. 51677093) and National Natural Science Foundation of China (NSFC) (No. 51777100).

We would also like to thank Dr. Lisha Peng (pls14@mails.tsinghua.edu.cn) for English writing assistance in the revised manuscript.

REFERENCES

[1]. R. B. Thompson, Generation of horizontally polarized shear waves in ferromagnetic materials using magnetostrictively coupled meander- coil electromagnetic transducers, Appl. Phys. Lett. 34 (1979) 175-177.
[2]. C. B. Thring, Y. Fan, R. S. Edwards, Multi-coil focused EMAT for characterisation of surface-breaking defects of arbitrary orientation, NDT&E Int. 88 (2017) 1-7,.
[3]. L. Kang, C. Zhang, S. Dixon, H. Zhao, S. Hill, M. Liu, Enhancement of ultrasonic signal using a new design of Rayleigh-wave electromagnetic acoustic transducer, NDT&E Int. 86 (2017) 36-43.
[4]. S. Wang, S. Huang, Y. Zhang, W. Zhao, Multiphysics Modeling of a Lorentz Force-Based Meander Coil Electromagnetic Acoustic Transducer via Steady-State and Transient Analyses, IEEE Sens. J. 16 (2016), 6641-6651.
[5]. N. Nakamura, K. Ashida, T. Takishita, H. Ogi, M. Hirao, Inspection of stress corrosion cracking in welded stainless steel pipe using point-focusing electromagnetic-acoustic transducer, NDT&E Int. 83 (2016) 88-93.
[6]. C. B. Thring, Y. Fan, R. S. Edwards, Focused Rayleigh wave EMAT for characterisation of surface-breaking defects, NDT&E Int. 81 (2016) 20-27.
[7]. Z. Wei, S. Huang, S. Wang, W. Zhao, Magnetostriction-Based Omni-Directional Guided Wave Transducer for High-Accuracy Tomography of Steel Plate Defects, IEEE Sens. J. 15 (2015) 6549-6558.
[8]. R. Dhayalan, K. Balasubramaniam, A hybrid finite element model for simulation of electromagnetic acoustic transducer (EMAT) based plate waves, NDT&E Int, 43 (2016) 519-526.
[9]. W. Ren, J. He, S. Dixon, K. Xu, Enhancement of EMAT's efficiency by using silicon steel laminations back-plate, Sens. Actuators, A. 274 (2018) 189-198.
[10]. C. Pei, P. Xiao, S. Zhao, Z. Chen, Development of a flexible film electromagnetic acoustic transducer for nondestructive testing, Sens. Actuators, A. 258 (2017) 68-73.
[11]. C. Pei, S. Zhao, P. Xian, Z. Chen, A modified meander-line-coil EMAT design for signal amplitude enhancement, Sens. Actuators, A. 247 (2016) 539-546.
[12]. S. Huang, W. Zhao, Y. Zhang, S. Wang, Study on the lift-off effect of EMAT, Sens. Actuators, A. 153 (2009) 218-221.
[13]. X. Jian, S. Dixon, K. Quirk, K. Grattan, Electromagnetic acoustic transducers for in- and out-of plane ultrasonic wave detection, Sens. Actuators, A. 148 (2008) 51-56.
[14]. X. Jian, S. Dixon, K. Grattan, R. Edwards, A model for pulsed Rayleigh wave and optimal EMAT design, Sens. Actuators, A. 128 (2006) 296-304.
[15]. S. Legendre, D. Massicotte, J. Goyette, et al, Neural classification of Lamb wave ultrasonic weld testing signals using wavelet coefficients, IEEE Trans. Instrum. Meas. 50 (2001) 672-678.
[16]. S. Legendre, D. Massicotte, J. Goyette, et al, Wavelet-transform-based method of analysis for Lamb-wave ultrasonic NDE signals, IEEE Trans. Instrum. Meas. 49 (2000) 524-530.
[17]. J. Silva, M. Wamzeller, P. Farias J. Neto, Development of Circuits for Excitation and Reception in Ultrasonic Transducers for Generation of Guided Waves in Hollow Cylinders for Fouling Detection, IEEE Trans. Instrum. Meas. 57 (2008) 1149-1153.
[18]. Petcher P A, Dixon S, Weld defect detection using PPM EMAT generated shear horizontal ultrasound, Ndt & E International, 74 (2015) 58-65.
[19]. H. M. Seung, C. Il Park, Y. Y. Kim, An omnidirectional shear-horizontal guided wave EMAT for a metallic plate, Ultrasonics, 69 (2016) 58–66.
[20]. X. Zhao, J. L. Rose, Guided circumferential shear horizontal waves in an isotropic hollow cylinder, The Journal of the Acoustical Society of America,115 (2004) 1912-1916.
[21]. S. Hill, S. Dixon, Frequency dependent directivity of periodic permanent magnet electromagneitc acoustic transducers, NDT&E Int. 62 (2014) 137–143.
[22]. Nurmalia, N. Nakamura, H. Ogi, M. Hirao, Detection of shear horizontal guided waves propagating in aluminum plate with thinning region, Jpn. J. Appl. Phys. 50 (2011) 07HC17.
[23]. P. Petcher, S. Burrows, S. Dixon, Shear horizontal (SH) ultrasound wave propagation around smooth corners, Ultrasonics, 54 (2014) 997-1004.
[24]. P. Petcher, S. Dixon. Weld defect detection using PPM EMAT generated shear horizontal ultrasound. NDT&E Int., 74 (2015) 58-65.
[25]. Z. Wei, S. Huang, S. Wang, et al. Magnetostriction-based omni-directional guided wave transducer for high-accuracy tomography of steel plate defects, IEEE Sens. J. 15 (2015), 6549-6558.
[26]. Y. Zhang, S. Huang, S. Wang, et al. Direction-controllable electromagnetic acoustic transducer for SH waves in steel plate based on magnetostriction, Progress in Electromagnetics Research M, 50 (2016) 151-160.

[27]. R. Ribichini, F. Cegla, P. B. Nagy, P. Cawley, Study and comparison of different EMAT configurations for SH wave inspection, IEEE Transactions on Ultrasonics, Ferroelectrics, and Frequency Control, 58 (2011) 2571-2581.
[28]. X. Song, G. Qiu, Optimization of a Focusable and Rotatable Shear-Wave Periodic Permanent Magnet Electromagnetic Acoustic Transducers for Plates Inspection, Sensors, 17 (2017) 2722.
[29]. H. Ogi, E. Goda, M. Hirao, Increase of Efficiency of Magnetostriction SH-Wave Electromagnetic Acoustic Transducer by Angled Bias Field: Piezomagnetic Theory and Measurement, Jpn. J. Appl. Phys. 42 (2003) 3020-3034.

Biographies

Hongyu Sun received the B.S degree from the Department of Renewable Energy, North China Electric Power University, Beijing, China, in 2015, and the master's degree from the department of Electrical and Electronic Engineering, North China Electric Power University, Beijing, China, in 2018.

He is currently pursuing the Ph.D. degree within the Department of Electrical Engineering, Tsinghua University. His major research interests include electromagnetic measurement, nondestructive evaluation, and plasma physics.

Songling Huang received the bachelor's degree in automatic control engineering from Southeast University, Nanjing, China, in 1991, and the Ph.D. degree in nuclear application technology from Tsinghua University, Beijing, China, in 2001.

He is currently a Professor within the Department of Electrical Engineering, Tsinghua University. His research interests include nondestructive evaluation and instrument techniques.

Qing Wang received the B.Eng. in electronic instrument and measurement technique from Beihang University, Beijing, China, in 1995, the M.Sc. degree in advanced manufacturing and materials from the University of Hull, Hull, U.K., in 1998, and the Ph.D. degree in manufacturing management from De Montfort University, Leicester, U.K., in 2001.

She is currently an Associate Professor in the School of Engineering and Computing Sciences, Durham University, Durham, U.K. Her research interests include electronic instruments and measurement, computer simulation, and advanced manufacturing technology.

Shen Wang received the bachelor's and Ph.D. degrees in electrical engineering from Tsinghua University, Beijing, China, in 2002 and 2008, respectively.

He is currently a Research Assistant within the Department of Electrical Engineering, Tsinghua University. His research interests include nondestructive testing and evaluation, and virtual instrumentation.

Wei Zhao received the bachelor's degree in electrical engineering from Tsinghua University, Beijing, China, in 1982, and the Ph.D. degree from the Moscow Power Engineering Institute Technical University, Moscow, Russia, in 1991.

He is currently a Professor within the Department of Electrical Engineering, Tsinghua University. His research interests include modern electromagnetic measurement and instrument techniques.